Short communication

Electrochemical synthesis of Ni−S/CeO$_2$ composite electrodes for hydrogen evolution reaction

Zhen Zheng [a], Ning Li [a,*], Chun-Qing Wang [b], De-Yu Li [a], Fan-Yu Meng [c], Yong-Ming Zhu [d], Qing Li [e], Gang Wu [e]

[a] School of Chemical Engineering and Technology, Harbin Institute of Technology, Harbin 150001, China
[b] State Key Laboratory of Advanced Welding Production Technology, Harbin Institute of Technology, Harbin 150001, China
[c] School of Municipal and Environmental Engineering, Harbin Institute of Technology, Harbin 150090, China
[d] Faculty of Applied Chemistry, Harbin Institute of Technology at Weihai, Weihai, 264209, China
[e] Materials Physics and Applications Division, Los Alamos National Laboratory, Los Alamos, NM 87545, USA

HIGHLIGHTS

► The correlation of synthesis−structure−activity is studied on Ni−S/CeO$_2$ coatings.
► The CeO$_2$ particles embedded in Ni−S matrix can increase the HER activity.
► The addition of CeO$_2$ particles can increase the sulphur content.
► The addition of CeO$_2$ particles can increase the amorphous components.

ARTICLE INFO

ABSTRACT

Ni−S/CeO$_2$ electrodes have been prepared by a composite electrodeposition technique using nickel sulfaminate bath containing suspended micro- or nano-sized CeO$_2$ particles. The composite electrodes exhibit a high activity for the hydrogen evolution reaction (HER) in alkaline solutions, most likely due to the synergistic effects between Ni and CeO$_2$, as well as the increased surface area of the electrodes upon addition of CeO$_2$ particles. It is found that the addition of CeO$_2$ particles can lead to an increase of the sulphur content, resulting in more amorphous structures in the composite coatings. The Ni−S/micro-CeO$_2$ composite electrode yields a higher HER activity than that measured with Ni−S/nano-CeO$_2$ electrode, which is 2.2 times higher than that on the Ni−S coating. The relevant discussion was provided to elucidate the promotional roles of CeO$_2$ particles in the composite electrodeposition process and corresponding HER activity.

© 2012 Published by Elsevier B.V.

1. Introduction

Hydrogen has the necessary properties to fulfil the role of a secondary source of energy that can be derived from the primary source by the decomposition of water [1,2]. Compared to other methods for hydrogen generation depending on the natural gas reforming or gasification of coal and petroleum coke, the water electrolysis technology is a sustainable method to produce hydrogen which relies only on renewable energy sources [3].

While the water electrolysis is of particular significance for hydrogen generation, its application is strictly limited by the high energy consumption caused by the considerable overpotential during the hydrogen evolution reaction (HER) [4]. In order to address this challenge, extensive studies have been dedicated to the development of advanced electrode materials for minimizing the HER overpotential. In principle, reasonably low HER overpotential can be achieved by increasing the real surface area and/or improving the intrinsic activity of the electrode materials [5−7]. Among the promising candidates for efficient HER electrode materials, the Ni-based materials have attracted a great attention due to their high activity and corrosion resistance in alkaline media [8]. In particular, Ni−S alloy is considered to be an excellent cathode material for the alkaline electrolysis relative to other binary alloys due to its easy preparation and low cost [9]. Importantly, amorphous Ni$_3$S$_2$ formed during the co-deposition process is able to accelerate the hydrogen adsorption and thus reduce the HER overpotential [10]. In addition,

the relatively large surface area of Ni–S alloy guarantees a high HER activity in water electrolysis [11,12].

On the other hand, the composite electrode materials derived from metallic matrix embedded by solid particles for HER have become a subject of increasing interest. For example, the Ni-based composite materials, such as Ni–MoO$_x$ [13,14] and Ni–TiO$_x$ [15] have been studied, offering a higher HER activity relative to Ni electrode. The incorporated particles in the Ni matrix are considered to be able to inhibit the growth of Ni grains and thus increase the surface area of the materials. Furthermore, the possible synergistic effects resulted from the interactions between induced particles and electrode coating, which may generate the intermetallic and/or amorphous compound, have been proved to further increase the intrinsic HER activity of the materials [16]. For the same reasons, some kinds of multicomponent materials based on Ni–S alloy have been reported in order to further enhance the HER activity [17–20]. However, the Ni–S composite electrodes with embedded solid particles for HER still remain insufficiently explored. In this work, the Ni–S/CeO$_2$ composite electrodes were prepared by an electrodeposition method in a nickel sulfamate bath containing CeO$_2$ particles. The thiourea was employed as the sulphur source, micro- and nano-sized CeO$_2$ particles were used for the composite preparation. The influences of the incorporation of CeO$_2$ particles into the Ni–S coating on the morphology and the phase composition of the coating were evaluated, and the effects of the particle size and the concentration of the CeO$_2$ particles on the HER activity were systematically investigated.

2. Experimental

The Ni–S/CeO$_2$ composite electrodes were deposited on 10×10 cm^2 mild steel plates by a composite electrodeposition method in an electrolyte containing 350 g L^{-1} Ni(NH$_2$SO$_3$)$_2$·4H$_2$O, 10 g L^{-1} NiCl$_2$·6H$_2$O, 30 g L^{-1} NH$_4$Cl, 100 g L^{-1} thiourea and micro-CeO$_2$ (5–7 μm) or nano-CeO$_2$ (20–30 nm) particles. The composite electrodeposition was conducted at a current density of 3.0 A dm^{-2} for about 1.0 h at 313 K with a magnetic stirring speed of 600 rpm. The as-obtained composite coatings with micro- or nano-sized CeO$_2$ particles were denoted as M1, M2, M3 or N1, N2, N3, when the concentration of CeO$_2$ was 5 g L^{-1}, 10 g L^{-1} and 15 g L^{-1}, respectively.

The morphology and crystalline structure of the composite coatings were investigated by SEM (FEI Quanta 200F) and XRD (D/max-rB), respectively. The CeO$_2$ content of the coatings was analyzed by EDX coupled with SEM, and the sulphur content was determined by the automatic elemental analyzer (Elementar Vario EL). Electrochemical measurements were carried out using a CHI 660 electrochemical workstation (CH Instrument, USA) in a standard three-electrode electrochemical cell at 298 K in a 1.0 M NaOH solution. Pt foil and Hg/HgO/OH$^-$ electrode (in 1.0 M NaOH) were used as the counter and the reference electrodes, respectively. Prior to steady-state polarization records, electrodes were first used for hydrogen evolution at a constant current density of 50 mA cm^{-2} for 1 h. Steady-state polarization curves were recorded at the scan rate of 1 mV s^{-1} (iR drop correction).

3. Results and discussion

The SEM images for the Ni–S and the Ni–S/CeO$_2$ composite electrodes are compared in Fig. 1. The microstructure of the Ni–S layer (Fig. 1a) illustrates the formation of complex cauliflower-like structure with a high porosity [12]. When micro-CeO$_2$ particles are embedded in the coating, a significantly flower-like morphology is observed with the M2 composite coating (Fig. 1c), suggesting a further increased surface area. When nano-CeO$_2$ particles are introduced in the synthesis, the crystalline sizes of the composite

coatings are much finer than that of the Ni–S coating. In the SEM image of the N3 composite coating (Fig. 1g), a uniform distribution of the nano-CeO$_2$ particles surrounding smaller Ni–S dendritic grains and eutectic is observed. The high magnification SEM images of the micro- and nano-CeO$_2$ particles in composites are shown in the Fig. 1h and i, respectively. Obviously, both micro- and nano-CeO$_2$ particles can enhance the porosity of Ni–S coating and thus increase the surface area of composite coatings.

Sulphur and CeO$_2$ content in different composite electrodes is compared in Fig. 2. The initial sulphur content in the Ni–S coating is about 12.8%. Upon the addition of CeO$_2$ particles, the sulphur content in the composite coatings increases, indicating that CeO$_2$ particles can accelerate the thiourea adsorption on the coating surface and this accelerating effect may benefit the formation of a finer microstructure. Interestingly, in all of the six composite electrodes, the S/Ni ratios keep a constant of 20%, which is higher than that (14.7%) in the Ni–S electrode. In fact, the formation of the amorphous phase with a more porous structure in Ni–S alloys is greatly dependent on the sulphur content and a large portion of amorphous phase has been demonstrated to be capable of achieving a higher HER activity [21].

The CeO$_2$ contents in the Ni–S composite layers are found to increase with a rise in the concentration of CeO$_2$ particles. Specifically, the CeO$_2$ contents in the composites derived from micro-CeO$_2$ particles are higher than those from the nano-CeO$_2$ particles. These results are in good agreement with the previous work reporting that the reduced particle size will lead to a lower corresponding element content in composites [22].

The phase composition and crystalline structure of the Ni–S coating, M2 and N2 composite coatings are studied using XRD (Fig. 3). The XRD pattern of Ni–S coating is dominated by the diffraction peaks of Ni (JCPDF No.65-2865) and no other species are detected, probably due to the fact that solution components adsorbed on the grain surface of Ni–S could not produce diffraction signals [12]. Although the Ni (220) diffraction peak can be observed clearly in the XRD pattern of the Ni–S coating, the same diffraction peak is much broader in those of the composite electrodes. Importantly, the Ni (111) diffraction peaks overlap with the Ni (200) diffraction peaks in XRD patterns of composite coatings, revealing an amorphous phase formed during the electrodeposition process. Specifically, the half-peak width of the Ni (111) diffraction peaks in Ni–S, M2 and N2 coatings are calculated to be 1.56°, 1.98° and 1.92°, respectively, corroborating the abundance of amorphous phase in composite coatings resulted from the higher sulphur content [23–25]. While the diffraction peaks of the CeO$_2$ particles in XRD pattern of M2 coating can be easily observed (JCPDF No. 43-1002), the CeO$_2$ diffraction peaks in the N2 electrode are less distinguishable, indicating a low CeO$_2$ content in the coating.

The HER steady-state linear polarization curves measured with the Ni, Ni–S/micro-CeO$_2$ and Ni–S/nano-CeO$_2$ electrodes are compared in Fig. 4. All the curves are characterized with a typical Tafel behaviour. Kinetic parameters for the HER (j_0 and Tafel slope b) are derived from the Tafel equation:

$$\eta_c = -\frac{2.3RT}{\alpha nF}\log j_0 + \frac{2.3RT}{\alpha nF}\log j \tag{1}$$

Here η_c is the cathode overpotential, R is the ideal gas constant, and T is the absolute temperature, α, n and F are the charge-transfer coefficient, number of electrons exchanged and the Faraday constant, respectively. And j_0 is the apparent exchange current density, which can be reasonably taken as a measurement of the catalytic efficiency [26,27].

It can be seen in Fig. 4a that the Ni–S coating shows higher HER activity than Ni coating and the activities are further improved upon
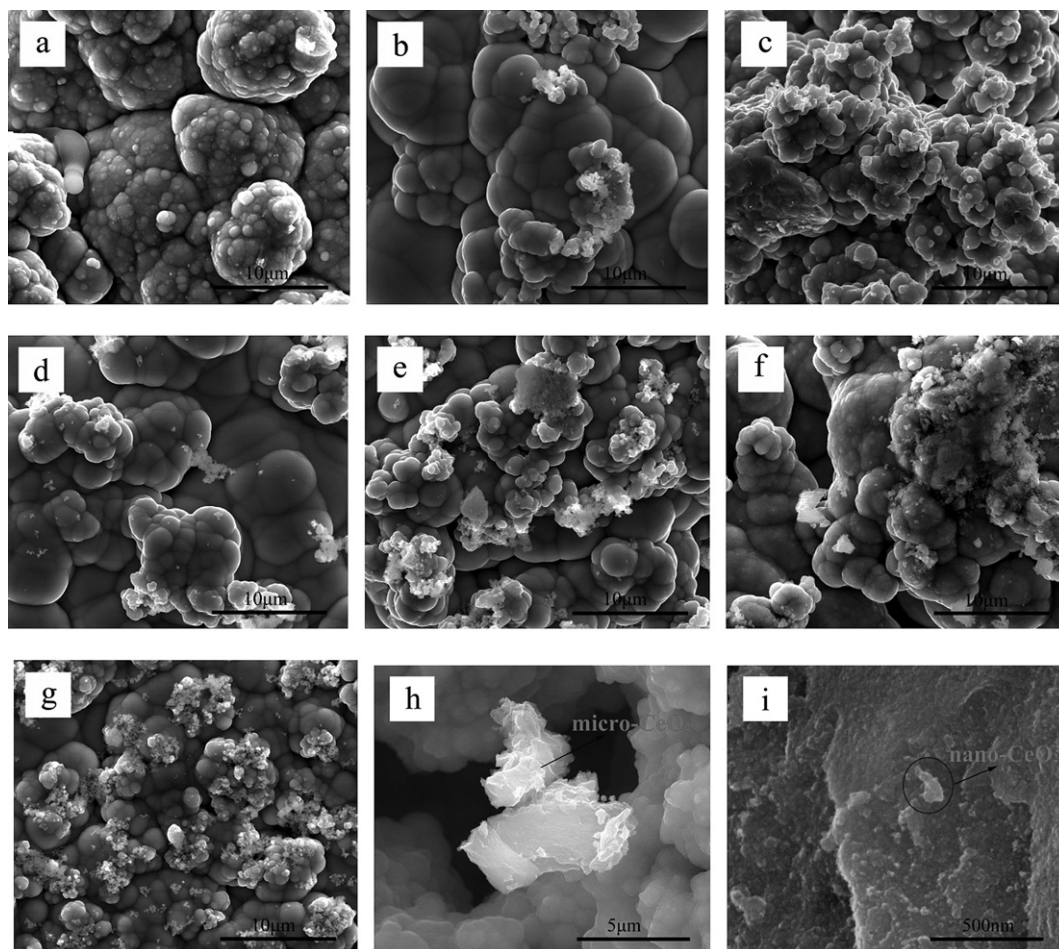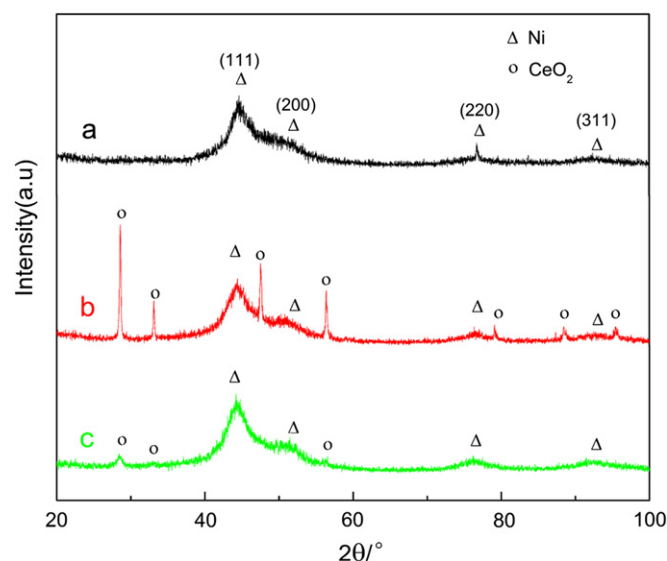
Fig. 1. SEM images of the Ni–S coating and Ni–S/CeO$_2$ composite coatings. (a) The Ni–S, (b) M1, (c) M2, (d) M3, (e) N1, (f) N2, (g) N3 composite coatings, (h) the composited micro-CeO$_2$ particle, (i) composited nano-CeO$_2$ particles.

the introduction of micro-CeO$_2$ particles into Ni–S coatings, with M2 electrode exhibits the highest catalytic activity for HER. The HER activities measured with nano-CeO$_2$ based composites (Fig. 4b) are also better than those on Ni–S coating, but independent on the CeO$_2$ concentrations used during the synthesis. The kinetic parameters of the Ni, Ni–S and composite electrodes are listed in the inset of Fig. 4. In good agreement with HER polarization plots, enhanced j_0 are observed on the Ni–S electrode and Ni–S/CeO$_2$ composite electrodes

relative to that on Ni coating. M2 and N2 composite electrodes exhibit the highest j_0 among Ni–S/micro-CeO$_2$ and Ni–S/nano-CeO$_2$ composite electrodes, which are 2.2 times and 1.9 times higher than that on the Ni–S coating, respectively. According to the above
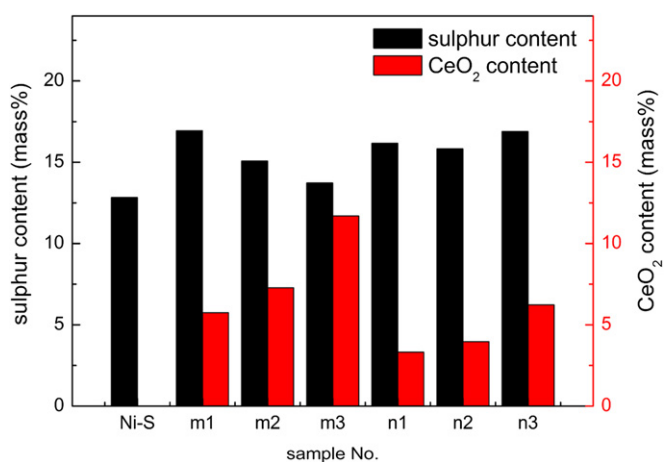
Fig. 2. Sulphur and CeO$_2$ content (mass %) in different composite electrodes.

Fig. 3. XRD patterns of the Ni–S coating and Ni–S/CeO$_2$ composite coatings. (a) The Ni–S, (b) M2, (c) N2 composite coatings.
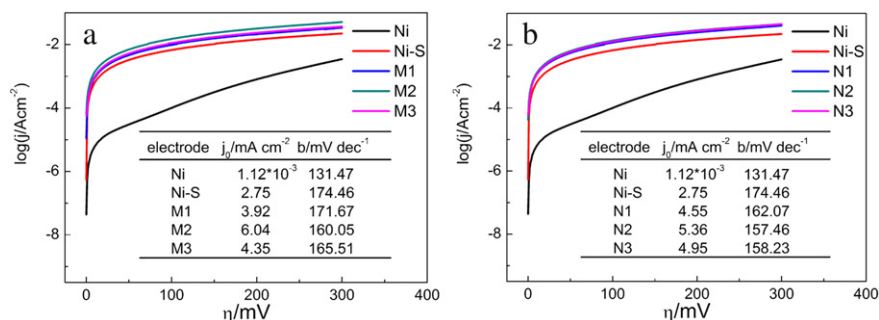
Fig. 4. Steady-state polarization curves and the result of the HER on the Ni, Ni—S and composite coatings (a. Ni—S/micro-CeO_2 and b. Ni—S/nano-CeO_2) in 1.0 M NaOH at 298 K.

analysis, it is evident that the composite electrodes possess a high HER activity, especially when micro-CeO_2 particles are used at an optimal content. The possible reasons account for the observed high HER activity should be related to the increased surface area of the composite electrodes due to the addition of CeO_2 particles, as evidenced by the SEM images of the composite electrodes. In addition, the increased sulphur content in the composite electrodes may improve the HER activity through the effect on the formation of the Ni—S amorphous phase [21]. Importantly, the HER intermediate product, i.e. H atom can easily adsorb on Ce atoms due to the presence of several half-filled and empty d orbitals. Hence, a possible synergetic effect may exist between CeO_2 and the Ni matrix, accelerating the formation of the H_{ads} and enhancing the HER activity [28,29]. It is probably the reason why M2 electrode with higher CeO_2 content shows better HER activity than Ni—S/nano-CeO_2 electrodes. However, it is worth noting that the ratio of sulphur to CeO_2 should be a key for HER in as-synthesized composite electrodes because the HER activity of M1 and M3 are slightly lower than Ni—S/nano-CeO_2 electrodes, even though the CeO_2 content in Ni—S/micro-CeO_2 electrodes are higher than those in Ni—S/nano-CeO_2 electrodes.

Tafel slope (b) is an important parameter and can provide insights into the HER mechanism on the electrodes. According to the Tafel equation (1), $b = 2.3RT/(\alpha F)$, thus the charge-transfer coefficient (α) that indicates the rate-determining step (RDS) can be calculated. The α of the Ni—S coating and composite electrodes are all measured to be between 0.33 and 0.37. Therefore, the RDS of HER on the studied composite electrodes may be the Volmer reaction or the Volmer reaction coupled with Heyrovsky reaction or Tafel reaction [30,31].
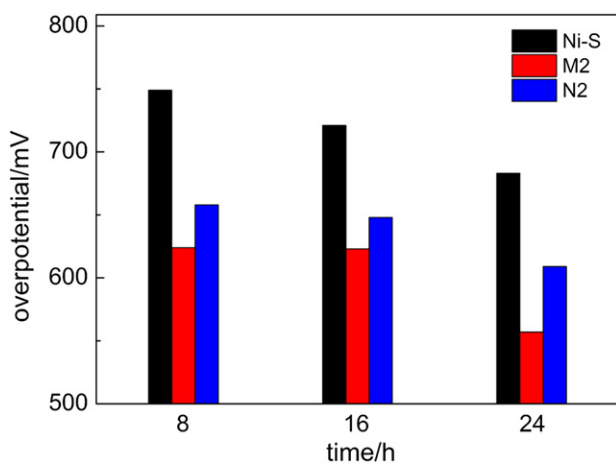
According to the steady-state linear polarization results, the addition of the CeO_2 particles in the Ni—S coating can increase the HER activity. The overpotentials of the developed Ni—S/CeO_2 composite electrodes in HER are further studied in a continuous electrolysis experiment. Fig. 5 shows the HER overpotentials of the Ni—S, M2 and N2 in 1.0 M NaOH solution at 298 K under a current density of 200 mA cm^{-2} for 24 h. It can be seen that M2 composite electrode reveals the lowest HER overpotential among all the three electrodes. These results are consistent with the steady-state linear polarization measurements.

4. Conclusions

The Ni—S composite electrodes containing micro- or nano-CeO_2 particles were prepared using a composite electrodeposition method for HER in alkaline solution. The best performing Ni—S/CeO_2 composite electrode was prepared from a solution containing 10 g L^{-1} micro-sized CeO_2. The measured HER activity is 2.2 times higher than that on Ni—S coating. The particle size and concentration of the CeO_2 particles are well correlated with the resulting morphology, crystalline structure and corresponding HER activities. It was found that the addition of CeO_2 particles can lead to an increase in the surface area and the sulphur content of the composite electrodes. Especially, the CeO_2 particles can accelerate the thiourea adsorption on the coating surface and this accelerating effect may benefit the formation of a finer microstructure, thus facilitating their HER activities. In addition, HER intermediates, such as H atom can easily adsorb on Ce atoms due to the presence of several half-filled and empty d orbitals. Hence, a possible synergetic effect may exist between CeO_2 and the Ni matrix, accelerating the formation of the H_{ads} and enhancing the HER activity.

References

[1] W.E. Winsche, K.C. Hoffman, F.J. Salzano, Science 180 (1973) 1325—1332.
[2] J. Greeley, T.F. Jaramillo, J. Bonde, I.B. Chorkendorff, J.K. Norskov, Nature Materials 5 (2006) 909—913.
[3] K. Zeng, D. Zhang, Progress in Energy and Combustion Science 36 (2010) 307—326.
[4] H. He, H. Liu, F. Liu, K. Zhou, Materials Letters 59 (2005) 3968—3972.
[5] I. Herraiz-Cardona, E. Ortega, L. Vázquez-Gómez, V. Pérez-Herranz, International Journal of Hydrogen Energy 36 (2011) 11578—11587.
[6] F.C. Crnkovic, S.A.S. Machado, L.A. Avaca, International Journal of Hydrogen Energy 29 (2004) 249—254.
[7] L. Chen, A. Lasia, Journal of the Electrochemical Society 139 (1992) 3458—3464.
[8] M.A. Domínguez-Crespo, A.M. Torres-Huerta, B. Brachetti-Sibaja, A. Flores-Vela, International Journal of Hydrogen Energy 36 (2011) 135—151.
[9] Q. Han, K. Liu, J. Chen, X. Wei, International Journal of Hydrogen Energy 28 (2003) 1207—1212.
[10] H. He, H. Liu, F. Liu, K. Zhou, Surface and Coatings Technology 201 (2006) 958—964.
[11] T.C. Wen, S.M. Lin, J.M. Tsai, Journal of Applied Electrochemistry 24 (1994) 233—238.
[12] R. Sabela, I. Paseka, Journal of Applied Electrochemistry 20 (1990) 500—505.
[13] N.V. Krstajić, L. Gajić-Krstajić, U. Lačnjevac, B.M. Jović, S. Mora, V.D. Jović, International Journal of Hydrogen Energy 36 (2011) 6441—6449.

Fig. 5. HER overpotential of the Ni, M-2 and N-2 electrodes as a function of electrolysis time.

[14] N.V. Krstajić, U. Lačnjevac, B.M. Jović, S. Mora, V.D. Jovi&cacute, International Journal of Hydrogen Energy 36 (2011) 6450–6461.

[15] R. Rashkov, M. Arnaudova, G. Avdeev, A. Zielonka, P. Jannakoudakis, A. Jannakoudakis, E. Theodoridou, International Journal of Hydrogen Energy 34 (2009) 2095–2100.

[16] G.J. Lu, P. Evans, G. Zangari, Journal of the Electrochemical Society 150 (2003) A551–A557.

[17] Q. Han, K. Liu, J. Chen, X. Li, X. Wei, International Journal of Hydrogen Energy 29 (2004) 243–248.

[18] Q. Han, Y. Jin, N. Pu, K. Liu, J. chen, X. Wei, Renewable Energy 35 (2010) 2627–2631.

[19] Q. Han, J. Chen, K. Liu, X. Wei, International Journal of Hydrogen Energy 33 (2008) 4495–4500.

[20] Q. Han, K. Liu, J. Chen, X. Wei, International Journal of Hydrogen Energy 34 (2009) 71–76.

[21] H. Vandenborre, P. Vermeiren, R. Leysen, Electrochimica Acta 29 (1984) 297–301.

[22] S.-C. Wang, W.-C.J. Wei, Materials Chemistry and Physics 78 (2003) 574–580.

[23] H. Ashassi-Sorkhabi, S.H. Rafizadeh, Surface and Coatings Technology 176 (2004) 318–326.

[24] J. Sun, T. Yang, G. Du, H. Liang, J. Bian, L. Hu, Applied Surface Science 253 (2006) 2066–2070.

[25] N.M. Martyak, K. Drake, Journal of Alloys and Compounds 312 (2000) 30–40.

[26] S. Trasatti, Journal of Electroanalytical Chemistry and Interfacial Electrochemistry 39 (1972) 163–184.

[27] M.P. Marceta Kaninski, S.M. Miulovic, G.S. Tasic, A.D. Maksic, V.M. Nikolic, International Journal of Hydrogen Energy 36 (2011) 5227–5235.

[28] Z. Zheng, N. Li, C.-Q. Wang, D.-Y. Li, Y.-M. Zhu, G. Wu, International Journal of Hydrogen Energy 37 (2012) 13921–13932.

[29] Z. Zheng, N. Li, C.-Q. Wang, D.-Y. Li, F.-Y. Meng, Y.-M. Zhu, Journal of Power Sources 222 (2013) 88–91.

[30] J.M. Jakšić, M.V. Vojnović, N.V. Krstaji&cacute, Electrochimica Acta 45 (2000) 4151–4158.

[31] A. Damian, S. Omanovic, Journal of Power Sources 158 (2006) 464–476.